RSC Advances

PAPER

View Article Online
View Journal | View Issue

Cite this: *RSC Adv.*, 2023, **13**, 1617

Carrier-free nanomedicines self-assembled from palbociclib dimers and Ce6 for enhanced combined chemo-photodynamic therapy of breast cancer†

Zheng Huang,[ab] Huaisong Hu,[a] Tong Xian,[a] Zhigang Xu,[a] Dianyong Tang,[a] Bochu Wang[b] and Yimei Zhang *[ab]

Palbociclib is the world's first CDK4/6 kinase inhibitor to be marketed. However, it is not effective in the treatment of triple negative breast cancer (TNBC) due to the loss of retinoblastoma protein expression. Thus, combinatorial chemotherapy is indispensable for TNBC treatment. Herein, a carrier-free nanomedicine self-assembled from palbociclib dimers and Ce6 for enhanced combined chemo-photodynamic therapy of breast cancer is reported. The dimeric prodrug (**Palb-TK-Palb**) was synthesized by conjugating two palbociclib molecules to the connecting skeleton containing a ROS-responsive cleavable thioketal bond. The **Palb-TK-Palb/Ce6 NP** co-delivery nanoplatform was prepared through the self-assembly of **Palb-TK-Palb**, Ce6 and DSPE-PEG2000. This novel carrier-free formulation as an efficient therapeutic agent showed efficient therapeutic agent loading capacity, high cellular uptake and huge therapeutic performance against breast cancer cells. The results of *in vitro* antitumor activity and cell apoptosis demonstrated that **Palb-TK-Palb/Ce6 NPs** presented a better inhibitory effect on the growth of cancer cells due to the palbociclib and Ce6 co-delivery nanomedicine-mediated synergistic chemo-photodynamic therapy. The IC_{50} values of **Palb-TK-Palb/Ce6 NPs** in MDA-MB-231 cells were around 1–2 μM and 2 μM and the **Palb-TK-Palb/Ce6 NPs** showed an increase in apoptosis up to 91.9%. In general, the carrier-free nanomedicine self-assembled from palbociclib dimers and Ce6 provides options for combinatorial chemo-photodynamic therapy.

Received 20th September 2022
Accepted 30th December 2022

DOI: 10.1039/d2ra05932k

rsc.li/rsc-advances

1. Introduction

According to Global Cancer Statistics 2020, breast cancer is the most commonly diagnosed cancer among women and remains the second principal cause of cancer-related death.[1] Among all subtypes of breast tumors, triple negative breast cancer (TNBC) is considered nearly fatal for its high metastatic capacity, relatively poor prognosis and lack of effective treatment options.[2,3] Currently, chemotherapy is the main treatment for early and late stage TNBC. Palbociclib is a specific inhibitor of cell cycle protein-dependent kinase 4/6 (CDK4/6). Recently, it has become a star drug for breast cancer, especially for estrogen receptor-positive breast cancer.[4] Since TNBC is short of retinoblastoma protein expression, which is critical for the response of CDK4/6 inhibitors, palbociclib is not very effective in the treatment of TNBC.[5] In addition, concomitant administration of palbociclib with cytotoxic paclitaxel or doxorubicin against TNBC had an antagonistic effect.[6,7] Even so, palbociclib is still able to inhibit the cyclin D3–CDK6 and reduce the flow of glucose-derived carbon into the pentose phosphate and serine synthesis pathways, leading to a significant increase of reactive oxygen species (ROS) level in tumor.[8] Preclinical evidence reveals that palbociclib can lead to tumor regression, resulting in a net decrease in tumor burden.[9,10] Palbociclib is now in clinical trials for treatment of TNBC patients who are overexpressing the androgen receptor (AR).[11,12] We therefore hypothesized that combination of chemotherapy mediated by palbociclib and photodynamic therapy (PDT) could produce a synergistic and enhanced effect against TNBC.

PDT uses photosensitizer (PS) to convert molecular oxygen into ROS with high cytotoxicity in cells and tissues under laser irradiation at specific wavelength, thereby inducing tumor cell necrosis and apoptosis to achieve the therapeutic purpose.[13–15] This therapy provides the advantages of high accuracy, good controllability, and low side effects on healthy tissues.[16,17] However, most photosensitizers have poor water solubility, poor stability and low intracellular accumulation in tumor cells, and these drawbacks limit their wide application in biological media.[18,19] The utilization of nanocarriers is the most common

[a]*National & Local Joint Engineering Research Center of Targeted and Innovative Therapeutics, Chongqing Key Laboratory of Kinase Modulators as Innovative Medicine, College of Pharmacy & International Academy of Targeted Therapeutics and Innovation, Chongqing University of Arts and Sciences, Chongqing 402160, China. E-mail: yimeizhang@cqwu.edu.cn*

[b]*Key Laboratory of Bio-theological Science and Technology of Ministry of Education, College of Bioengineering, Chongqing University, Chongqing, 400045, China*

† Electronic supplementary information (ESI) available. See DOI: https://doi.org/10.1039/d2ra05932k

strategy to improve the water solubility of photosensitizers.[20] Nevertheless, disadvantages including low drug loading efficacy, complicated synthesis carriers induced bio-insafety *etc.*, restrict the practical use of carrier-based nanomedicines.[21,22] Meanwhile, it is also encouraged to use minimum amount of excipient as possible the large-scale industry.[23–25]

Recently, carrier-free nanomedicines were proposed for efficient cancer therapy. Among them, drug–drug conjugates especially drug dimers nano-assemblies were the most commonly used.[26,27] Drug dimers are prodrugs by conjugating two same therapeutic agents directly or *via* a short stimuli-responsive linker.[28,29] As a result, the carrier-free nanomedicines formed by the self-assembly of drug dimers in the absence of non-therapeutic carriers demonstrate several outstanding properties such as high biosecurity and free from the carrier-induced immunogenicity and toxicities, simple drug compositions and preparation procedures and high drug loading rates.[30] Dimers of podophyllotoxin (PPT),[31] SN-38,[32] CPT[33] and PTX[34,35] with different linkers have exhibited high drug delivery potential. However, palbociclib-based dimers have been rarely reported to date.[22] In addition to its unique properties, the drug dimers could also co-assemble with other therapeutic agents for synergistic treatments. For instance, the oxidation-responsive cabazitaxel dimers (CTX-S-CTX) were self-assembled with PPa to obtain pCTX-S-CTX/PPa nanodrugs for self-enhancing chemo-photodynamic therapy.[36] The PPa-generated ROS together with the endogenous ROS synergistically facilitated the release of CTX.

Herein, inspired by the background and findings above, we designed and developed a carrier-free nanomedicines self-assembled with ROS-responsive palbociclib dimer prodrug and photosensitizer Chlorin E6 (Ce6) for combined chemo-photodynamic therapy of TNBC. Drug dimers (**Palb-TK-Palb**) through conjugating palbociclib with ROS-responsive cleavable thioketal linkages was synthesized. The prodrugs could be fabricated into drug nanoparticles (**Palb-TK-Palb/Ce6 NPs**) with Ce6 *via* reprecipitation method. This novel carrier-free nanoplatform could significantly improve the water solubility and stability of palbociclib and Ce6, thereby increasing effective accumulation at cancer cells sites. When the co-delivery systems were irradiated with a 660 nm laser in breast cancer cells, ROS was generated, and the endogenous ROS together with Ce6-generated ROS synergistically triggered the cleavage of **Palb-TK-Palb** for controlled release of palbociclib to perform chemotherapy. Moreover, the generated ROS also performed PDT to promote combined therapeutic effects. Overall, the carrier-free nanomedicine system might be considered an effective strategy to enhance synergistic effect and improve the therapeutic efficiency of TNBC treatment.

2. Materials and methods

All chemicals and reagents were obtained commercially and were used as received. Chlorin E6 (Ce6) was purchased from Macklin Biochemical Technology Co., LTD (Shanghai, China). 1,2-Distearoyl-*sn*-glycero-3-phosphoethanolamine-*N*-[methoxy(polyethylene glycol)-2000] (ammonium salt) (DSPE-PEG2000) was obtained from Avanti Polar Lipids (USA). 3-(4,5-Dimethylthiazol-2-yl)-2,5-diphenyltetrazolium bromide (MTT) was purchased from Sangon Biotech (Shanghai, China). Hoechst 33342, Total Glutathione Assay Kit, Lipid Peroxidation MDA Assay Kit, Calcein/PI Cell Viability/Cytotoxicity Assay Kit and Annexin V-FITC Apoptosis Detection Kit were purchased from Beyotime Biotechnology (Shanghai, China). Human triple-negative breast cancer MDA-MB-231 cell line was purchased from the Cobioer Biosciences (Nanjing, China). The products were purified by Biotage Isolera™ Spektra Systems. ^{1}H and ^{13}C NMR were performed on a Bruker 400 spectrometer.

2.1. Synthesis of Palb-TA-Palb

2-(7-Azabenzotriazol-1-yl)-*N*,*N*,*N*′,*N*′-tetramethyluronium hexafluorophosphate (HATU, 160.0 mg, 0.42 mmol) and *N*,*N*-diisopropylethylamine (DIPEA, 79.7 mg, 0.63 mmol) were added sequentially to a mixture dichloromethane solution (20 mL) of TK–COOH (3,3′-(propane-2,2-diylbis(sulfanediyl))dipropionic acid, 25.1 mg, 0.10 mmol) at 0 °C. After stirring for 30 min, palbociclib hydrochloride (100.2 mg, 0.21 mmol) was added to the mixture. The resulting mixture was stirred for 24 h at room temperature and then was concentrated by rotatory evaporator. After purification by column chromatography over silica gel eluting with a gradient of CH_3OH/CH_2Cl_2 (0 to 10%), **Palb-TA-Palb** was obtained as yellow powder (yield: 87%).

^{1}H-NMR ($CDCl_3$, 400 MHz): δ/ppm 8.85 (s, 2H, –CH–), 8.31–8.21 (m, 2H, –CH–), 8.11–8.03 (m, 2H, –CH–), 7.35–7.43 (m, 2H, –CH–), 5.92–5.81 (m, 2H, –CH–), 3.87–3.78 (m, 4H, $-CH_2-$), 3.73–3.63 (m, 4H, $-CH_2-$), 3.24–3.12 (m, 8H, $-CH_2-$), 2.95–2.91 (m, 4H, $-CH_2-$), 2.72–2.63 (m, 4H, $-CH_2-$), 2.55 (s, 6H, $-CH_3$), 2.38 (s, 6H, $-CH_3$), 2.36–2.31 (m, 2H, –CH–), 2.13–2.00 (m, 4H, $-CH_2-$), 1.94–1.84 (m, 4H, $-CH_2-$), 1.79–1.65 (m, 8H, $-CH_2-$), 1.64 (s, 6H, $-CH_3$). ^{13}C NMR ($CDCl_3$, 100 MHz): δ/ppm 202.5, 169.7, 161.4, 158.4, 157.9, 157.1, 155.6, 145.6, 143.1, 141.6, 131.1, 113.9, 108.0, 56.2, 54.2, 49.9, 45.3, 41.5, 33.2, 31.5, 30.9, 28.1, 25.8. HRMS (ESI): *m*/*z* calculated for $C_{59}H_{70}N_{14}O_6S_2$ $[M + H]^+$ 1111.5117; found 1111.5105.

2.2. Synthesis of Palb-TK-Palb

A solution of 4-nitrophenyl chloroformate (411.4 mg, 2.10 mmol) in CH_2Cl_2 (2 mL) was dropwise added to a mixture dichloromethane solution (20 mL) of TK–OH (3,3′-(propane-2,2-diylbis(sulfanediyl))bis(propan-1-ol), 25.1 mg, 0.11 mmol) and DIPEA (516.1 mg, 4.00 mmol) at 0 °C. The resulting mixture was stirred overnight at room temperature and concentrated by rotatory evaporator. The crude product was dissolved in DMF (6 mL) immediately and palbociclib hydrochloride (100.1 mg, 0.21 mmol) was added. The resulting mixture was stirred for 24 h at room temperature and then was concentrated by rotatory evaporator. After purification by column chromatography over silica gel eluting with a gradient of CH_3OH/CH_2Cl_2 (0 to 10%), **Palb-TK-Palb** was obtained as yellow powder (yield: 62%).

^{1}H-NMR ($CDCl_3$, 400 MHz): δ/ppm 8.91 (s, 2H, –CH–), 8.26–8.10 (m, 4H, –CH–), 7.39–7.31 (m, 2H, –CH–), 5.93–5.81 (m, 2H, –CH–), 4.27–4.16 (m, 4H, $-CH_2-$), 3.73–3.62 (m, 8H, $-CH_2-$), 3.23–3.10 (m, 8H, $-CH_2-$), 2.75–2.66 (m, 4H, $-CH_2-$), 2.55 (s, 6H, $-CH_3$), 2.39 (s, 6H, $-CH_3$), 2.37–2.32 (m, 2H, –CH–), 2.13–2.03 (m, 4H, $-CH_2-$), 2.00–1.93 (m, 4H, $-CH_2-$), 1.93–1.83 (m, 4H, $-CH_2-$), 1.76–1.65 (m, 4H, $-CH_2-$), 1.62–1.60 (m, 4H, $-CH_2-$), 1.59 (s, 6H, $-CH_3$). ^{13}C NMR ($CDCl_3$, 100 MHz): δ/ppm 202.5, 161.4, 158.2, 157.3, 155.6, 155.2, 145.8, 143.3, 141.8, 137.0, 130.8, 127.0, 113.6, 107.6, 64.6, 56.3, 54.2, 43.6, 31.5, 31.0, 29.2, 28.1, 26.8, 25.7. HRMS (ESI): m/z calculated for $C_{59}H_{74}N_{14}O_8S_2$ $[M + H]^+$ 1171.5328; found 1171.5341.

2.3. Synthesis of Palb-CC-Palb

A solution of 4-nitrophenyl chloroformate (411.4 mg, 2.10 mmol) in CH_2Cl_2 (2 mL) was dropwise added to a mixture dichloromethane solution (20 mL) of CC–OH (nonane-1,9-diol, 25.1 mg, 0.10 mmol) and DIPEA (516.2 mg, 4.01 mmol) at 0 °C. The resulting mixture was stirred overnight at room temperature and concentrated by rotatory evaporator. The crude product was dissolved in DMF (6 mL) immediately and palbociclib hydrochloride (100.2 mg, 0.21 mmol) was added to the mixture. The resulting mixture was stirred for 24 h at room temperature and then was concentrated by rotatory evaporator. After purification by column chromatography over silica gel eluting with a gradient of CH_3OH/CH_2Cl_2 (0 to 10%), **Palb-CC-Palb** was obtained as yellow powder (yield: 71.2%).

^{1}H-NMR ($CDCl_3$, 400 MHz): δ/ppm 8.89 (s, 2H, –CH–), 8.27–8.14 (m, 2H, –CH–), 8.16–8.09 (m, 2H, –CH–), 7.41–7.33 (m, 2H, –CH–), 5.93–5.83 (m, 2H, –CH–), 4.17–4.06 (m, 4H, $-CH_2-$), 3.72–3.63 (m, 8H, $-CH_2-$), 3.22–3.08 (m, 8H, $-CH_2-$), 2.55 (s, 6H, $-CH_3$), 2.39 (s, 6H, $-CH_3$), 2.38–2.33 (m, 2H, –CH–), 2.13–1.97 (m, 4H, $-CH_2-$), 1.94–1.83 (m, 4H, $-CH_2-$), 1.73–1.61 (m, 12H, $-CH_2-$), 1.37–1.28 (m, 10H, $-CH_2-$). ^{13}C NMR ($CDCl_3$, 100 MHz): δ/ppm 202.6, 161.4, 158.2, 157.2, 155.2, 145.7, 143.4, 141.8, 136.9, 130.8, 127.0, 113.7, 107.6, 65.8, 63.0, 54.2, 49.8, 43.6, 31.5, 29.7, 29.5, 29.3, 29.2, 29.1, 29.0, 28.9, 28.1, 25.9, 25.7. HRMS (ESI): m/z calculated for $C_{59}H_{74}N_{14}O_8S_2$ $[M + H]^+$ 1107.5887; found 1107.5881.

2.4. Preparation of NPs

The **NP-1–NP-7** were formed with **Palb-TK-Palb** and different weight DSPE-PEG2000. 2.0 mg **Palb-TK-Palb** and DSPE-PEG2000 (0%, 10%, 15%, 20%, 25%, 27.5%, 30% weight of **Palb-TK-Palb**) were dissolved in 1 mL of DMSO. Then, the mixture was added dropwise to 10 mL of deionized water under stirring vigorously. After 2 h, DMSO and the not self-assembled **Palb-TK-Palb** were removed through dialysis against distilled water (MWCO = 1000). **Palb-TK-Palb NPs**, **Palb-TA-Palb NPs** and **Palb-CC-Palb NPs** were also prepared similarly with 0.75 mg DSPE-PEG2000 (27.5% weight of dimer prodrug).

The Ce6 loaded nanoparticles (**Palb-TA-Palb/Ce6 NPs**, **Palb-TK-Palb/Ce6 NPs** and **Palb-CC-Palb/Ce6 NPs**) were also prepared similarly. Starting feeding amount of NPs was 2.0 mg **Palb-TK-Palb** (**Palb-TA-Palb** or **Palb-CC-Palb**), 0.75 mg DSPE-PEG2000 and 2.0 mg Ce6. The preparation of **SPC/Ce6 NPs** as controls was the same as the above, except that **SPC/Ce6 NPs** were prepared by using 1-palmitoyl-2-linoleoyl-*sn*-glycero-3-phosphocholine (SPC) rather than dimer prodrug.

The concentration of Ce6 and palbociclib was determined by the UV absorbance at 660 nm and 366 nm according to the standard calibration curve of Ce6 and palbociclib in DMSO.

2.5. Size and morphology of NPs

The size of NPs with different proportions was first characterized by dynamic light scattering (DLS) using Zetasizer Nano ZSP instrument (Malvern Instruments Ltd) at room temperature. Then, the size and morphology of **Palb-TK-Palb NPs** and **Palb-TK-Palb/Ce6 NPs** were measured by DLS and TEM (JEM-1400plus system (JEOL, Japan)).

The storage stability of **Palb-TK-Palb/Ce6 NPs** was examined. After storing at 4 °C for 1, 5 and 12 days, the particle size was examined by DLS. The **Palb-TK-Palb/Ce6 NPs** were incubated under 100 mM H_2O_2 or PBS (0.05 M, pH 5.0) at 37 °C for 48 h. The changes in size were monitored by DLS.

2.6. The drug loading content (DLC) and drug loading efficiency (DLE)

In brief, a certain amount of NPs was lyophilized and weighed. The concentration of palbociclib and Ce6 in NPs was determined through UV-vis spectra according to the standard curve of palbociclib and Ce6. The DLCs and DLEs were calculated by the following equation:

$$\text{DLC (100\%)} = (\text{weight of drug in NPs/weight of NPs}) \times 100\%$$

$$\text{DLE (100\%)} = (\text{weight of drug in NPs/weight of added drug}) \times 100\%$$

2.7. Cell culture

Medium consisting of DMEM and 10% FBS was used to culture the human triple negative breast cancer MDA-MB-231 cells. MDA-MB-231 cells were kept at 37 °C in a humidified environment with 5% CO_2.

2.8. Cell uptake

MDA-MB-231 cells were seeded into 96-well microplates (PerkinElmer) and cultured at 37 °C for 24 h. Cells were treated with free Ce6, **SPC/Ce6 NPs**, and **Palb-TK-Palb/Ce6 NPs** (2 μM equivalent Ce6) for 4 h. Hoechst 33342 (λ_{ex} = 346 nm, λ_{em} = 460 nm) was used to stained the cell nuclei for 10 min. Then, the cells were washed and photographed by the high content analysis system.

Flow cytometry was also used to observe the uptake of Ce6-loaded NPs. MDA-MB-231 cells were seeded into 6-well plates and incubated at 37 °C for 24 hours. After 4 hours of incubation, cells were washed, collected and suspended in PBS. Untreated cells were used as controls. The fluorescent intensity of Ce6 was measured by flow cytometry (BD, USA).

2.9. Cellular ROS detection

DCFH-DA was used as an ROS indicator to determine the intracellular ROS production. MDA-MB-231 cells were seeded into CellCarrier 96-well microplates (PerkinElmer) and cultured at 37 °C for 24 h. Cells were incubated with different formulations for 4 h. Cells were washed and cultured in fresh medium with DCFH-DA ($\lambda_{ex} = 488$ nm, $\lambda_{em} = 525$ nm) for 30 min. Then, the cells were washed with PBS and fresh medium was added. After 660 nm laser irradiation (20 mW cm^{-2}) for 1 min, the cells were photographed by the high content analysis system.

2.10. Measurement of cellular lipid ROS levels

MDA-MB-231 cells were seeded into 6 cm dishes and cultured at 37 °C for 24 h. Cells were incubated with different formulations (2 μM equivalent Ce6, 3.6 μM equivalent palbociclib) for 4 h. The cell culture medium was renewed with fresh medium. After 660 nm laser irradiation (20 mW cm^{-2}, 2 min), the cells were further incubated for 20 h at 37 °C. Cells were collected and assayed utilizing the Lipid Peroxidation MDA Assay Kit (Beyotime Biotechnology, China).

2.11. Chemo-photodynamic synergistic therapy

The synergistic therapeutic effect of **Palb-TK-Palb/Ce6 NPs** against MDA-MB-231 cells using MTT method was evaluated. MDA-MB-231 cells were seeded into 96-well plates and cultured at 37 °C for 24 h. Cells were incubated with different formulations for 4 h. The cell culture medium was renewed with fresh medium. For dark group, the cells were cultured in dark for another 20 h. For laser group, after irradiated with 660 nm laser (20 mW cm^{-2}) for 1 min, the cells were cultured in dark for another 20 h. The cells were photographed by the high content analysis system. Then, cells were further incubated with MTT solution for 4 h. After removing the medium, 200 μL of DMSO was added to each well. The absorbance at 570 nm was measured with the microplate reader (Bio-Tek, Winooski, VT, USA). The cells without any treatments were used as the control.

2.12. Cell apoptosis

MDA-MB-231 cells were seeded into 6 cm dishes and cultured at 37 °C for 24 h. Cells were incubated with different formulations (2 μM equivalent Ce6). After 4 h incubation cells were irradiated with 660 nm laser (20 mW cm^{-2}) for 1 min. The non-treated cells were used as controls. Cells were collected and assayed utilizing Annexin V-FITC Apoptosis Detection Kit (Beyotime Biotechnology, China).

2.13. Live/dead cell staining

MDA-MB-231 cells were seeded into CellCarrier 96-well microplates (PerkinElmer) and cultured at 37 °C for 24 h. Cells were incubated with different formulations (2 μM equivalent Ce6). Cells were washed with PBS and fresh medium was added after 4 hours of incubation. After 660 nm laser irradiation (20 mW cm^{-2}) for 1 min and the cells were incubated for 20 h. Then, cells were stained with calcein-AM and PI for 30 min. The cells were photographed by the high content analysis system.

3. Results and discussion

3.1. Design and synthesis of palbociclib dimer prodrug

The synthetic route of the palbociclib dimers bridged with a ROS-responsive thioketal linker is shown in Scheme 1. Briefly, **Palb-TA-Palb** containing a thioketal and linked by an amide bond was synthesized *via* a one-pot amide condensation reaction using palbociclib and TK–COOH, which was synthesized according to our previous work.[37] Carbamate bond connected **Palb-TK-Palb** and **Palb-CC-Palb** with or without thioketal were synthesized by a similar method, except that their linkage skeletons were first prepared as chloroformates using TK–OH (3,3′-(propane-2,2-diylbis(sulfanediyl))bis(propan-1-ol)) and nonane-1,9-diol. The synthesized products were confirmed by ^{1}H NMR spectrum, ^{13}C NMR spectrum and mass spectrum (Fig. S1–S9†).

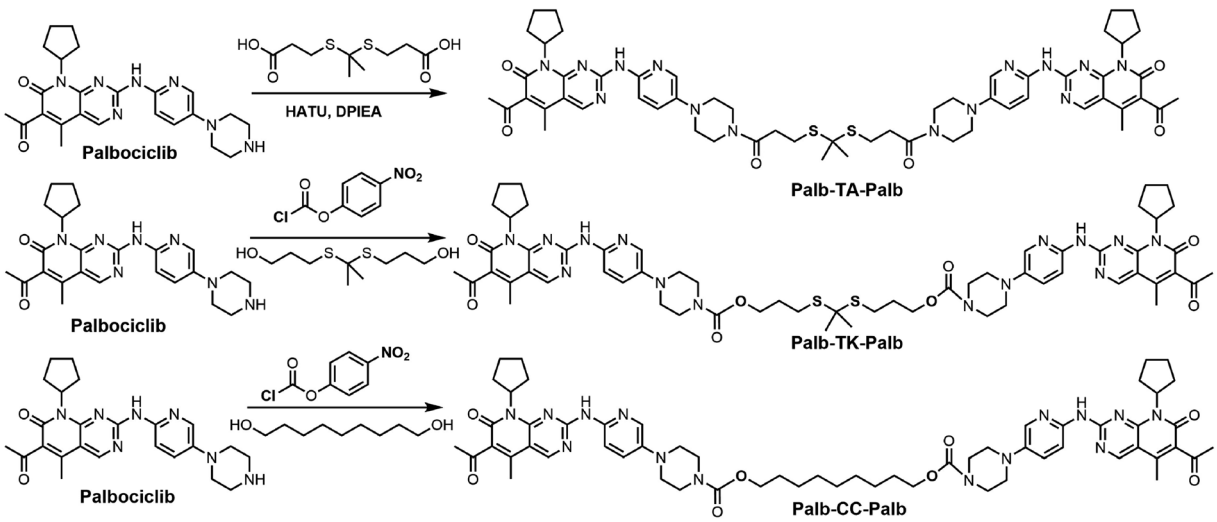

Scheme 1 Synthetic routes of target palbociclib dimer prodrugs.

3.2. Preparation and characterization of carrier-free nanomedicines

Since drug dimers could be fabricated into drug nanoparticles (NPs) and further co-assemble with other drugs to form multi-functional nanomedicines, the self-assembly abilities of **Palb-TK-Palb** were subsequently investigated. DSPE-PEG2000 was added to improve the performance of nanoassemblies for improving the function of NPs and the weight content of DSPE-PEG2000 was meticulously optimized. The different **Palb-TK-Palb NPs** were prepared using the reprecipitation method[22] with 0, 10%, 15%, 20%, 25%, 27.5% and 30% of DSPE-PEG2000, respectively. It was found that **Palb-TK-Palb NPs** with 27.5% DSPE-PEG2000 exhibited minimal PDI and maximum count rate (Table S1†). Therefore, we will choose this composition ratio to prepare Ce6-loaded nanoparticles in the subsequent experiments.

Then, dynamic light scattering (DLS) and transmission electron microscopy (TEM) assays were utilized to characterize the particle size and morphology of the obtained NPs. The results revealed that the particle size of **Palb-TK-Palb NPs** was around 70 nm. After encapsulating Ce6, the sizes of **Palb-TK-Palb/Ce6 NPs** was slightly increased to about 80 nm (Fig. 1A). The findings indicated that Ce6 could be effectively encapsulated by **Palb-TK-Palb NPs** to form chemotherapeutic agent palbociclib and photosensitizer Ce6 co-delivery carrier-free nanomedicines. TEM images showed that both prepared NPs were generally spherical in shape with good monodispersity (Fig. 1B and C). The difference in particle size of nanoparticles measured by DLS and TEM might be caused by the different experimental conditions: the particle sizes determined by DLS were examined in the hydrated state in solution, while TEM revealed the morphology of the micelles in the dehydrated state.[38] In addition, the **Palb-TK-Palb/Ce6 NPs** had good stability and the particle size remained unchanged within two weeks (Fig. S10A†). Subsequently, the ROS and pH responsive behavior of the **Palb-TK-Palb/Ce6 NPs** were investigated since the **Palb-TK-Palb** dimers had thioketal bond and carbamate linkers. As shown in Fig. S10B,† after treatment with 100 mM H_2O_2 or pH = 5.0 PBS for 48 h incubation, the both particle sizes were increased significantly and new peaks appeared, which can be on account of the degradation of the sensitive linker groups triggered by ROS or pH, resulting in the destruction of **Palb-TK-Palb/Ce6 NPs**. The DLS graphs (as shown Fig. S10†) of different nanomaterials display components with hydrodynamic diameters larger than 100 nm. This might be agglomerated aggregates of free (not aggregated) DSPE-PEG2000 strands.[29] The possible ROS-triggered degradation mechanism of **Palb-TK-Palb** was further studied by HR-MS. It was found that the peaks of **Palb-SH** and **Palb-SO_3H** were found in HR-MS spectrum after **Palb-TK-Palb** was incubated with 200 mM H_2O_2 for 48 h (Fig. S11A†). Therefore, we provided the possible ROS-triggered degradation mechanism of **Palb-TK-Palb** (Fig. S11B†).

After verifying the successful response of the **Palb-TK-Palb/Ce6 NPs** to ROS and pH, we further employed a dialysis method to confirm the *in vitro* palbociclib and Ce6 release behavior from **Palb-TK-Palb/Ce6 NPs** in a high concentration ROS and simulated acidic environment (Fig. 1D and E). Both palbociclib and Ce6 are released rarely and slowly under physiological conditions. In contrast, the release rate was dramatically accelerated under pH = 5.0 and 200 mM H_2O_2 conditions. The release of palbociclib and Ce6 reached the maximum at 2 and 10 h, respectively. In contrast, it was found that palbociclib

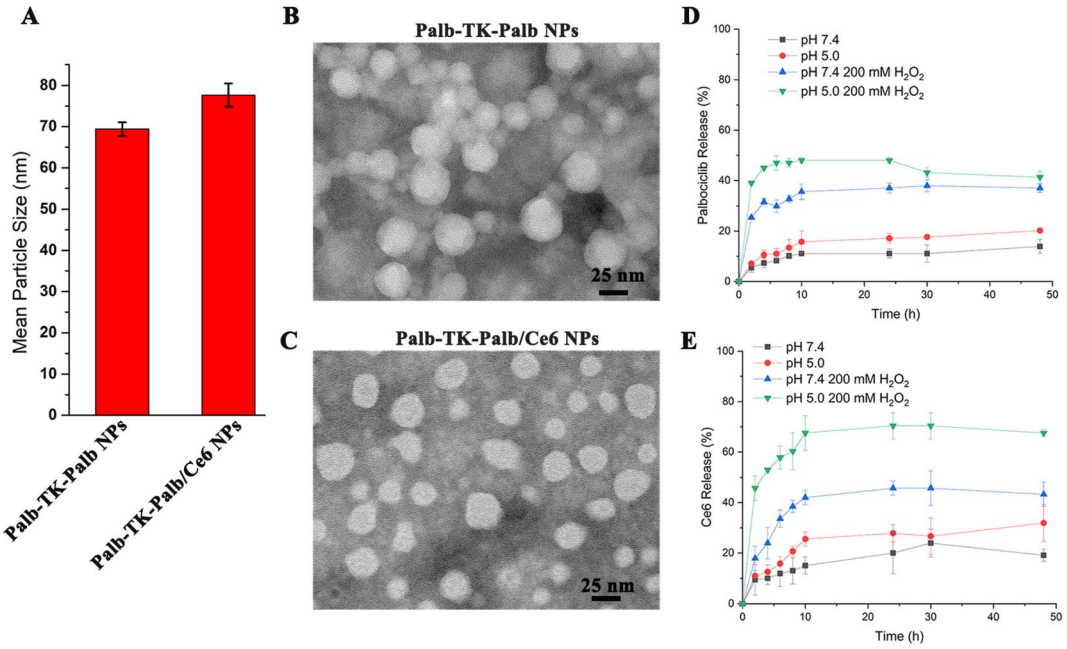

Fig. 1 The mean particle size of **Palb-TK-Palb NPs** and **Palb-TK-Palb/Ce6 NPs** measured by DLS (A). The TEM images of **Palb-TK-Palb NPs** (B) and **Palb-TK-Palb/Ce6 NPs** (C). The release profiles of palbociclib (D) and Ce6 (E) from **Palb-TK-Palb/Ce6 NPs** under pH = 7.4 PBS buffer solution or in a high concentration ROS and simulated acidic environment. Data are shown as mean ± SD (n = 3).

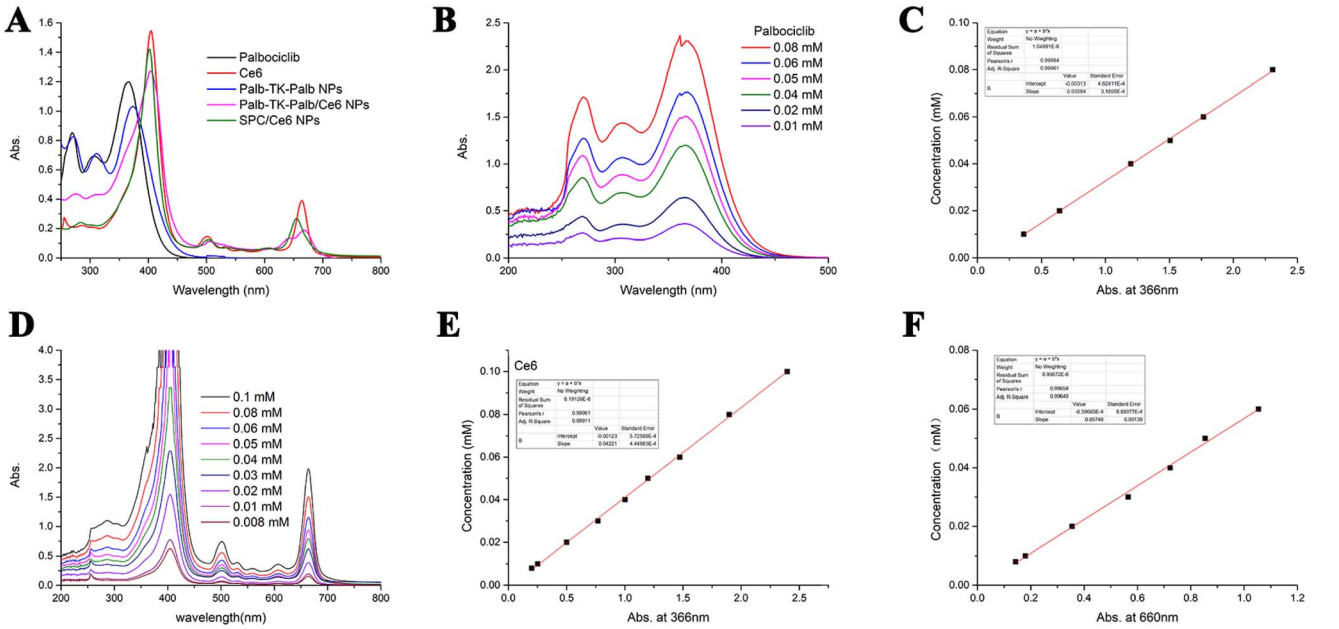

Fig. 2 (A) UV-vis spectra of palbociclib, Ce6, **Palb-TK-Palb NPs**, **Palb-TK-Palb/Ce6 NPs** and **SPC/Ce6 NPs**. (B) UV-vis spectra of palbociclib at various concentrations. (C) The standard curves of palbociclib. (D) UV-vis spectra of Ce6 at various concentrations. (E and F) The standard curves of Ce6 at 366 nm or at 660 nm.

released moderately after treatment with low pH or H_2O_2 for 48 h incubation. This result could be explained by the fact that the thioketone and carbamate bond are stable in physiological conditions (pH = 7.4) and easily destroyed in ROS and acidic conditions. This demonstrated that **Palb-TK-Palb/Ce6 NPs** could maintain the superior stability under physiological conditions control drug release in the cancer cell microenvironment.

Next, the spectroscopic properties of palbociclib and Ce6 in DMSO, **Palb-TK-Palb NPs**, **Palb-TK-Palb/Ce6 NPs** and **SPC/Ce6 NPs** in water were studied with the UV-vis spectrometer (Fig. 2A), in which the palbociclib and Ce6 showed a absorption peak at 270 and 366 nm, 404 and 660 nm, respectively. Both palbociclib and Ce6 showed concentration-dependent absorbance intensity (Fig. 2B and D). The loading capacities of palbociclib and Ce6 in **Palb-TK-Palb/Ce6 NPs** were determined to be 39.66% ± 1.24% and 33.91% ± 1.66% by using the standard curves measured by UV-vis spectrometer (Fig. 2C, E and F). The **Palb-TK-Palb/Ce6 NPs** had the highest DLC of palbociclib and a moderate DLC of Ce6 among three nanoparticles (Table 1). The high drug-loading capacity suggested that the co-delivery **Palb-TK-Palb/Ce6** carrier-free nanoplatform are capable of encapsulating both palbociclib and Ce6 efficiently.

Table 1 The drug loading content (DLC) of **Palb-TA-Palb/Ce6 NPs**, **Palb-TK-Palb/Ce6 NPs** and **Palb-CC-Palb/Ce6 NPs**

Nanoparticle	DLC of palbociclib (%)	DLC of Ce6 (%)
Palb-TA-Palb/Ce6 NPs	24.71 ± 2.61	29.32 ± 1.22
Palb-TK-Palb/Ce6 NPs	39.67 ± 1.24	33.91 ± 1.66
Palb-CC-Palb/Ce6 NPs	33.51 ± 2.25	36.00 ± 2.64

3.3. Cellular uptake efficiency

Before systematically investigating the bioactive properties of Ce6-loaded carrier-free nanomedicines, the cytotoxicity of different nanoparticles against MDA-MB-231 breast cancer cells were preliminarily examined. All of **Palb-TA-Palb**, **Palb-TK-Palb** and **Palb-CC-Palb NPs** showed no obvious cytotoxicity to MDA-MB-231 cells before encapsulating Ce6 even the concentration of palbociclib was high as 10 μM (Fig. S12A†), indicating the high biosecurity and free from the carrier-induced toxicities. Thus avoiding the toxic and side effects on normal tissues under non-light conditions. When exposed to 660 nm laser irradiations for 1 min, both **Palb-TA-Palb/Ce6** and **Palb-CC-Palb/Ce6 NPs** also revealed little cytotoxicity (Ce6 concentration: 0.1–1 μM). In contrast, **Palb-TK-Palb/Ce6 NPs** showed a moderate phototoxicity and the cell viability reduced to 60% at 1 μM of Ce6 (Fig. S12B†). Therefore, the subsequent experiments were conducted using **Palb-TK-Palb/Ce6 NPs** formulation due to the weak phototoxicity against breast cancer cells mediated by **Palb-TA-Palb/Ce6** and **Palb-CC-Palb/Ce6 NPs**.

Subsequently, the confocal laser scanning microscopy (CLSM) and flow cytometry were used to investigate the cellular uptake ability of different formulations. It was found that **Palb-TK-Palb/Ce6 NPs** can fully enter the cells at 2 h incubation and the cellular uptake did not increase when incubation time was longer than 4 h (Fig. S13†). Therefore, the cellular uptake of Ce6, **Palb-TK-Palb/Ce6 NPs** and **SPC/Ce6 NPs** after 4 h incubation was further studied. As shown in Fig. 3A, almost no red fluorescent signal of Ce6 appeared mediated by free Ce6 due to its poor aqueous solubility and moderate red fluorescent signal appeared treated by **SPC/Ce6 NPs**, which was used as control. In contrast, a considerable amount of the red fluorescent signal

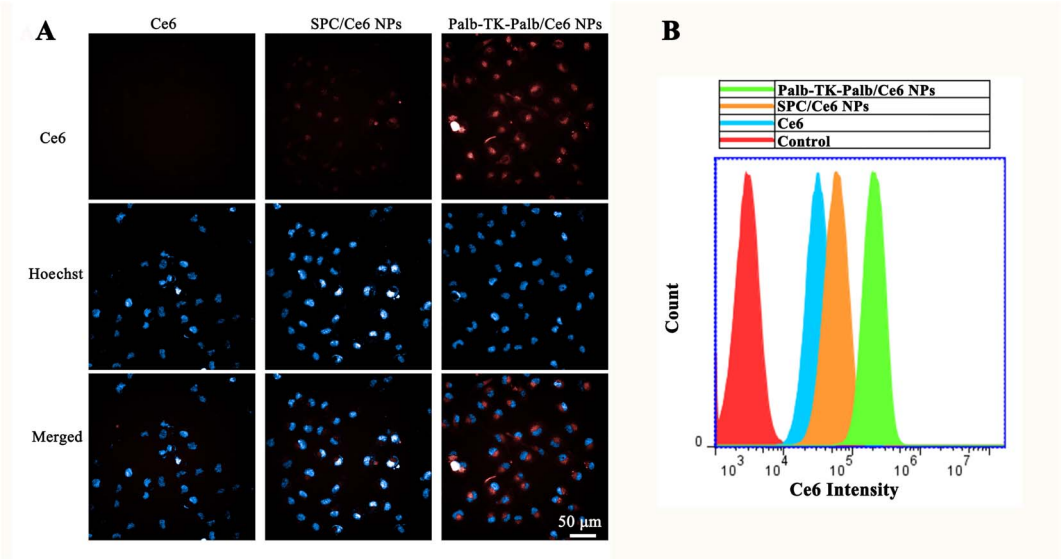

Fig. 3 *In vitro* cellular uptake ability of Ce6, **Palb-TK-Palb/Ce6 NPs** and **SPC/Ce6 NPs**. (A) Images of the MDA-MB-231 cells treated with different formulations for 4 h captured by high content analysis system-Operetta CLS™. (B) Flow cytometry measurement of MDA-MB-231 cells treated with different samples for 4 h.

could be observed after treated by **Palb-TK-Palb/Ce6 NPs**, which was consistent with the results obtained by flow cytometry (Fig. 3B), indicating high cellular uptake of **Palb-TK-Palb/Ce6 NPs**. The results suggested that drug dimers co-assemble with Ce6 could improve its water solubility and cellular internalization, which is necessary for the following delivery procedure.

3.4. Intracellular ROS generation

Since palbociclib could induce a significant increase of ROS level in tumor when reducing the flow of glucose-derived carbon into the pentose phosphate and serine synthesis pathways,[8] it encouraged us to survey intracellular ROS generation capability of MDA-MB-231 cells after treated with different formulations using the DCFH-DA fluorescent probe. As shown in Fig. 4A, ignorable green fluorescence was observed in MDA-MB-231 cells (control), Ce6-treated and palbociclib-treated cells, suggesting that free Ce6 or palbociclib alone could produce enough ROS because of the low cellular uptake efficiency. Neither **Palb-TK-Palb NPs** nor **SPC/Ce6 NPs** induced to produce sufficient amount of green fluorescence. As a comparison, the cells treated with **Palb-TK-Palb/Ce6 NPs** showed obviously green fluorescence, indicating that a significant quantity of ROS was

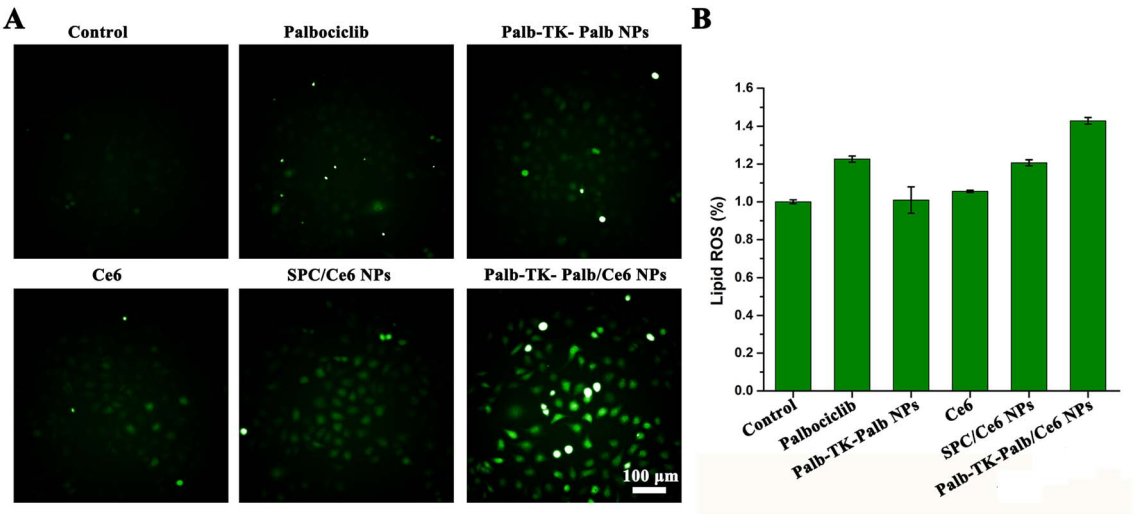

Fig. 4 Intracellular ROS generation capacity. (A) Confocal fluorescence images of MDA-MB-231 cells treated with 2 μM palbociclib, Ce6, **Palb-TK-Palb NPs**, **SPC/Ce6 NPs** and **Palb-TK-Palb/Ce6 NPs** under 660 nm laser irradiations (20 mW cm^{-2}) for 1 min. (B) The intracellular lipoperoxide levels in MDA-MB-231 cells incubated after treatment with different formulations for 24 h under 660 nm laser irradiations (20 mW cm^{-2}, 1 min). Data are shown as mean ± SD ($n = 3$).

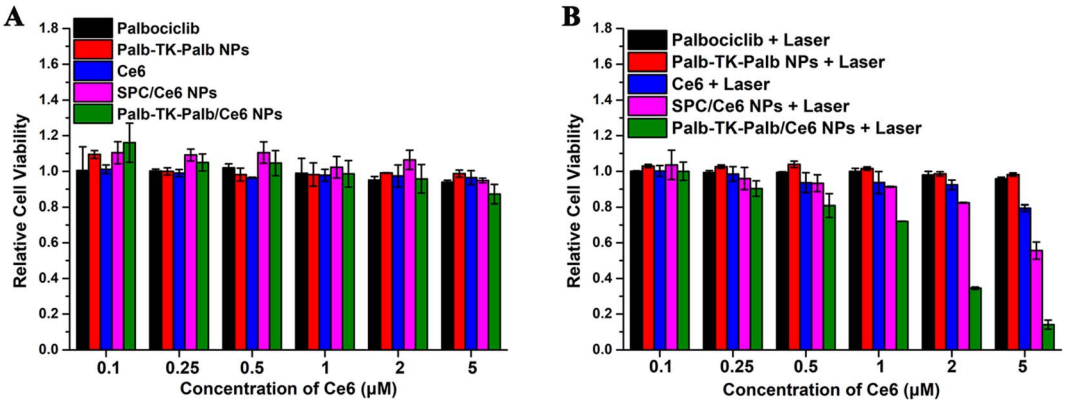

Fig. 5 Cytotoxicity of palbociclib, Ce6, **Palb-TK-Palb NPs**, **SPC/Ce6 NPs** and **Palb-TK-Palb/Ce6 NPs** at various concentrations against MDA-MB-231 cells without (A) and with (B) 660 nm laser irradiations (20 mW cm^{-2}, 1 min) after incubation for 24 h. Data are shown as mean ± SD (n = 3).

generated under light irradiation. This is mainly attributed to the good cellular internalization ability of **Palb-TK-Palb/Ce6 NPs** and synergistic ROS generation of palbociclib and Ce6-induced PDT.

The lipid ROS levels were further detected using thiobarbituric acid (TBA) as the probe because the severity of lipid peroxidation is an important indicator of oxidative stress. The results showed that the treatment with different groups except **Palb-TK-Palb/Ce6 NPs** had no significant change in lipid peroxidation levels. **Palb-TK-Palb/Ce6 NPs** had led to a 40% increase of lipid peroxidation levels in cancer cells, suggesting most intense oxidative stress occurred in MDA-MB-231 cells, which attributed to its high intracellular ROS generation ability of **Palb-TK-Palb/Ce6 NPs** and the subsequent oxidative stress response.

3.5. Chemo-photodynamic synergistic cytotoxicity

Then, the antitumor effect of combined chemo-photodynamic therapy mediated by carrier-free nanomedicines was further evaluated using the MTT assay *in vitro*. It was found that all the samples showed no cytotoxicity against MDA-MB-231 cells without light irradiations when the Ce6 concentrations gradually raised from 0.1–5 μM (Fig. 5A). Interestingly, the free palbociclib and Ce6, **Palb-TK-Palb NPs** also showed no significant cytotoxicity with light irradiations (Fig. 5B), suggesting that the anti-tumor effect of the alone therapeutic agent is not

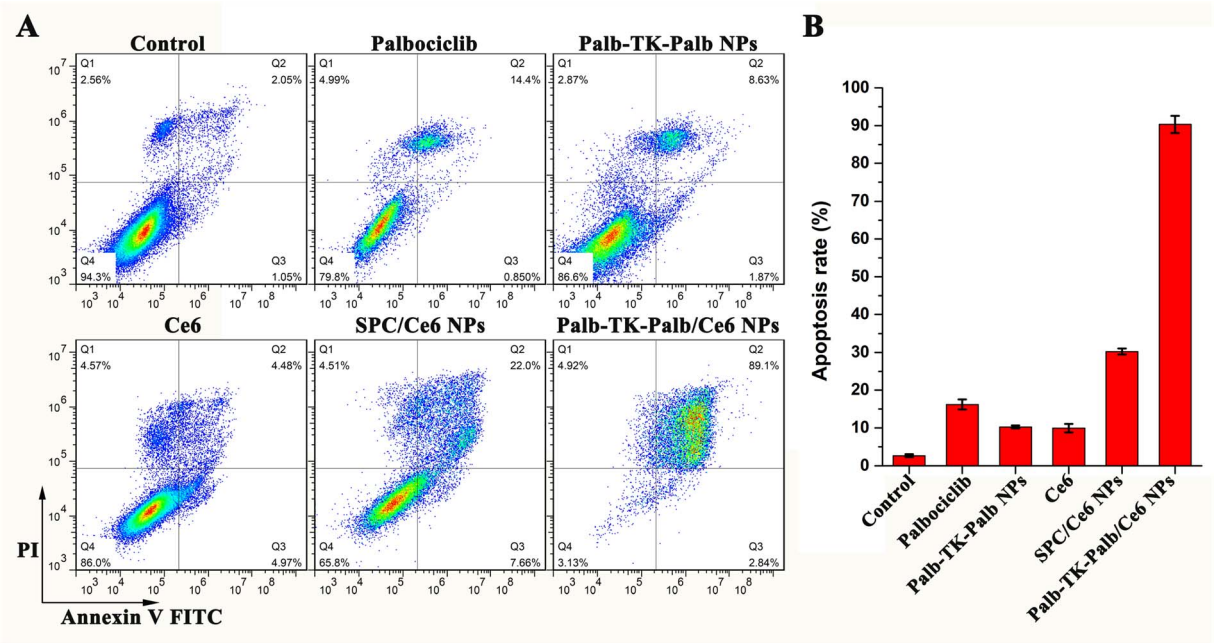

Fig. 6 Annexin V-FITC/PI-based apoptosis analysis (A) of MDA-MB-231 cells treated with palbociclib, Ce6, **Palb-TK-Palb NPs**, **SPC/Ce6 NPs** and **Palb-TK-Palb/Ce6 NPs** at concentration of 2 μM with laser irradiation (20 mW cm^{-2}, 1 min). The apoptosis rate following treatment with various samples (B).

satisfactory. In contrast, **SPC/Ce6 NPs** and **Palb-TK-Palb/Ce6 NPs** revealed dose-dependent cytotoxicity in MDA-MB-231 cells. When exposed to light (660 nm, 20 mW cm^{-2}, 1 min), the cell viability of the **Palb-TK-Palb/Ce6 NPs** group decreased from 100% to 10% (Ce6 concentration: 0.1–5 μM), which is much lower than that of the **SPC/Ce6 NPs** group (100% to 60%). These findings together suggest that the effective encapsulation of Ce6 and the synergistic effect of palbociclib-induced chemotherapy and Ce6-mediated photodynamic therapy are the keys to the high antitumor effect of **Palb-TK-Palb/Ce6 NPs**. The half-maximal inhibitory concentrations (IC_{50}) values of **Palb-TK-Palb/Ce6 NPs** against MDA-MB-231 cells was around 1–2 μM. In addition, the pronounced cancer cells inhibition effect of **Palb-TK-Palb/Ce6 NPs** was also consistently supported by the cell live/death imaging results (Fig. S14†). The above results demonstrated that **Palb-TK-Palb/Ce6 NPs** has the best inhibitory effect on the growth of cancer cells due to the palbociclib and Ce6 co-delivery nanomedicines-mediated synergistic chemo-photodynamic therapy.

3.6. Cell apoptosis

The flow cytometry analysis with Annexin V-FITC/PI staining was subsequently utilized to further investigate cell apoptosis, which was induced by different formulations. As shown in Fig. 6, after the MDA-MB-231 cells treated with 2 μM of palbociclib, **Palb-TK-Palb NPs**, Ce6, **SPC/Ce6 NPs** and **Palb-TK-Palb/Ce6 NPs** under laser irradiation for 1 min, the apoptosis rate was 15.3%, 10.5%, 9.5%, 30.0% and 91.9%, respectively. Moreover, the **Palb-TK-Palb/Ce6 NPs** were found to cause the late apoptosis (89.1%) and necrosis (4.9%) of cells. Under the same conditions, the **Palb-TK-Palb/Ce6 NPs** induced a much greater degree of cell apoptosis than the **Palb-TK-Palb NPs** and **SPC/Ce6 NPs**, suggesting that **Palb-TK-Palb/Ce6 NPs** co-assemble with palbociclib and Ce6 had stronger cytotoxicity as a result of synergetic chemo-photodynamic therapy. These results of *in vitro* antitumor activity and cell apoptosis collectively indicated the huge potential of **Palb-TK-Palb/Ce6 NPs** for breast cancer treatment.

4. Conclusions

In summary, we have designed and synthesized a series of drug dimers by coupling two palbociclib molecules with different connection linkers containing a ROS-sensitive thioketal bond. The carrier-free nanomedicines (**Palb-TK-Palb/Ce6 NPs**) were constructed by co-assembling drug dimers with photosensitizer Ce6. To further stabilize nanoparticle and endow passive targeting ability, DSPE-PEG2000 was introduced. The co-delivery nanoplatform exhibited efficient loading capacity for palbociclib and Ce6, ROS-stimulus response ability and high cellular uptake efficiency. In addition, the high cancer cells accumulation ability of **Palb-TK-Palb/Ce6 NPs** further guaranteed the highest cancer cells inhibition rate among other groups. The cell viability, cell apoptosis, and calcein-AM/PI staining experiments all indicated that enhanced cell cytotoxicity and combined chemo-photodynamic therapy effects have been achieved and the IC_{50} values of **Palb-TK-Palb/Ce6 NPs** in MDA-MB-231 breast cancer cells was around 1–2 μM. We believe that the co-delivery carrier-free nanoparticles self-assembled from palbociclib dimers and Ce6 have great advantage over conventional nanoparticle and will contribute to combinatorial cancer therapy.

Conflicts of interest

There are no conflicts to declare.

Acknowledgements

This work was financially supported by the National Natural Science Foundation of China (No. 21907012), Chongqing Natural Science Foundation (No. cstc2020jcyj-msxmX0908), Science and Technology Research Program of Chongqing Municipal Education Commission (No. KJQN202201324 and KJZD-K202201307), Special Funding for Postdoctoral Research Projects of Chongqing Human Resources and Social Security Bureau (No. 2021XM3094) and Science & Technology Research Program of Chongqing University of Arts and Sciences (No. R2018SBX12 and R2018SCH09). We thank Dr Zhi-Gang Xu for polishing the English language and style.

References

1 H. Sung, J. Ferlay, R. L. Siegel, M. Laversanne, I. Soerjomataram, A. Jemal and F. Bray, *Ca-Cancer J. Clin.*, 2021, **71**, 209–249.
2 X. Sun, M. Wang, M. Wang, X. Yu, J. Guo, T. Sun, X. Li, L. Yao, H. Dong and Y. Xu, *Front. Oncol.*, 2020, **10**, 428.
3 Z. Wang, Q. Jiang and C. Dong, *Cancer Biol. Med.*, 2020, **17**, 44–59.
4 R. S. Finn, M. Martin, H. S. Rugo, S. Jones, S. A. Im, K. Gelmon, N. Harbeck, O. N. Lipatov, J. M. Walshe, S. Moulder, E. Gauthier, D. R. Lu, S. Randolph, V. Diéras and D. J. Slamon, *N. Engl. J. Med.*, 2016, **375**, 1925–1936.
5 T. Yamamoto, N. Kanaya, G. Somlo and S. Chen, *Breast Cancer Res. Treat.*, 2019, **174**, 615–625.
6 A. K. McClendon, J. L. Dean, D. B. Rivadeneira, J. E. Yu, C. A. Reed, E. Gao, J. L. Farber, T. Force, W. J. Koch and E. S. Knudsen, *Cell Cycle*, 2012, **11**, 2747–2755.
7 C. A. Clark, H. B. Gupta, G. Sareddy, S. Pandeswara, S. Lao, B. Yuan, J. M. Drerup, A. Padron, J. Conejo-Garcia, K. Murthy, Y. Liu, M. J. Turk, K. Thedieck, V. Hurez, R. Li, R. Vadlamudi and T. J. Curiel, *Cancer Res.*, 2016, **76**, 6964–6974.
8 H. Wang, B. N. Nicolay, J. M. Chick, X. Gao, Y. Geng, H. Ren, H. Gao, G. Yang, J. A. Williams, J. M. Suski, M. A. Keibler, E. Sicinska, U. Gerdemann, W. N. Haining, T. M. Roberts, K. Polyak, S. P. Gygi, N. J. Dyson and P. Sicinski, *Nature*, 2017, **546**, 426–430.
9 W. Ji, W. Zhang, X. Wang, Y. Shi, F. Yang, H. Xie, W. Zhou, S. Wang and X. Guan, *Cell Death Dis.*, 2020, **11**, 760.
10 D. W. Fry, P. J. Harvey, P. R. Keller, W. L. Elliott, M. Meade, E. Trachet, M. Albassam, X. Zheng, W. R. Leopold,

N. K. Pryer and P. L. Toogood, *Mol. Cancer Ther.*, 2004, **3**, 1427–1438.
11 I. Galiana, B. Lozano-Torres, M. Sancho, M. Alfonso, A. Bernardos, V. Bisbal, M. Serrano, R. Martínez-Máñez and M. Orzáez, *J. Controlled Release*, 2020, **323**, 624–634.
12 N. C. Turner, J. Ro, F. André, S. Loi, S. Verma, H. Iwata, N. Harbeck, S. Loibl, C. Huang Bartlett, K. Zhang, C. Giorgetti, S. Randolph, M. Koehler and M. Cristofanilli, *N. Engl. J. Med.*, 2015, **373**, 209–219.
13 J. Xu, S. Yu, X. Wang, Y. Qian, W. Wu, S. Zhang, B. Zheng, G. Wei, S. Gao, Z. Cao, W. Fu, Z. Xiao and W. Lu, *ACS Nano*, 2019, **13**, 10242–10260.
14 S. Chakrabortty, B. K. Agrawalla, A. Stumper, N. M. Vegi, S. Fischer, C. Reichardt, M. Kögler, B. Dietzek, M. Feuring-Buske, C. Buske, S. Rau and T. Weil, *J. Am. Chem. Soc.*, 2017, **139**, 2512–2519.
15 W. Lv, Z. Zhang, K. Y. Zhang, H. Yang, S. Liu, A. Xu, S. Guo, Q. Zhao and W. Huang, *Angew. Chem., Int. Ed.*, 2016, **55**, 9947–9951.
16 X. Duan, C. Chan, N. Guo, W. Han, R. R. Weichselbaum and W. Lin, *J. Am. Chem. Soc.*, 2016, **138**, 16686–16695.
17 S. S. Lucky, K. C. Soo and Y. Zhang, *Chem. Rev.*, 2015, **115**, 1990–2042.
18 J. F. Lovell, T. W. B. Liu, J. Chen and G. Zheng, *Chem. Rev.*, 2010, **110**, 2839–2857.
19 L. Cheng, C. Wang, L. Feng, K. Yang and Z. Liu, *Chem. Rev.*, 2014, **114**, 10869–10939.
20 K. Han, Q. Lei, S.-B. Wang, J.-J. Hu, W.-X. Qiu, J.-Y. Zhu, W.-N. Yin, X. Luo and X.-Z. Zhang, *Adv. Funct. Mater.*, 2015, **25**, 2961–2971.
21 S.-Y. Qin, A.-Q. Zhang, S.-X. Cheng, L. Rong and X.-Z. Zhang, *Biomaterials*, 2017, **112**, 234–247.
22 L.-H. Liu and X.-Z. Zhang, *Prog. Mater. Sci.*, 2022, **125**, 100919.
23 Y. Xiang, C. Liu, L. Chen, L. Li and Y. Huang, *Adv. Ther.*, 2021, **4**, 2000261.
24 X. Cui, J. Zhao, Z. Mohmood and C. Zhang, *Chem. Rec.*, 2016, **16**, 173–188.
25 S. Tran, P.-J. DeGiovanni, B. Piel and P. Rai, *Clin. Transl. Med.*, 2017, **6**, 44.
26 Y. Liu, N. Wen, K. Li, M. Li, S. Qian, S. Li, T. Jiang, T. Wang, Y. Wu and Z. Liu, *Mol. Pharmaceutics*, 2022, **19**, 805–818.
27 S. Li, X. Shan, Y. Wang, Q. Chen, J. Sun, Z. He, B. Sun and C. Luo, *J. Controlled Release*, 2020, **326**, 510–522.
28 P. Huang, D. Wang, Y. Su, W. Huang, Y. Zhou, D. Cui, X. Zhu and D. Yan, *J. Am. Chem. Soc.*, 2014, **136**, 11748–11756.
29 S. Bai, L.-L. Yang, Y. Wang, T. Zhang, L. Fu, S. Yang, S. Wan, S. Wang, D. Jia, B. Li, P. Xue, Y. Kang, Z.-J. Sun and Z. Xu, *Small*, 2020, **16**, 2000214.
30 L. Huang, S. Zhao, F. Fang, T. Xu, M. Lan and J. Zhang, *Biomaterials*, 2021, **268**, 120557.
31 Y. Ikuta, Y. Koseki, T. Murakami, M. Ueda, H. Oikawa and H. Kasai, *Chem. Lett.*, 2013, **42**, 900–901.
32 H. Kasai, T. Murakami, Y. Ikuta, Y. Koseki, K. Baba, H. Oikawa, H. Nakanishi, M. Okada, M. Shoji, M. Ueda, H. Imahori and M. Hashida, *Angew. Chem., Int. Ed.*, 2012, **51**, 10315–10318.
33 Q. Pei, X. Hu, Z. Li, Z. Xie and X. Jing, *RSC Adv.*, 2015, **5**, 81499–81501.
34 Q. Pei, X. Hu, S. Liu, Y. Li, Z. Xie and X. Jing, *J. Controlled Release*, 2017, **254**, 23–33.
35 Z. Wang, M. Zhuang, T. Sun, X. Wang and Z. Xie, *Bioorg. Med. Chem. Lett.*, 2017, **27**, 2493–2496.
36 S. Zhang, Z. Wang, Z. Kong, Y. Wang, X. Zhang, B. Sun, H. Zhang, Q. Kan, Z. He, C. Luo and J. Sun, *Theranostics*, 2021, **11**, 6019–6032.
37 Y.-M. Zhang, M. Xia, R. Ao, L.-X. Gao, Y. Tang, J.-H. Huang, Y.-F. Luo, Z.-Z. Chen, B.-C. Wang and Z. Huang, *Nanomaterials*, 2021, **11**, 2875.
38 W.-J. Yi, Q.-F. Zhang, J. Zhang, Q. Liu, L. Ren, Q.-M. Chen, L. Guo and X.-Q. Yu, *Acta Biomater.*, 2014, **10**, 1412–1422.